Self-organizing motors divide active liquid droplets

Kimberly L. Weirich[a,b], Kinjal Dasbiswas[a,c], Thomas A. Witten[a,d], Suriyanarayanan Vaikuntanathan[a,e], and Margaret L. Gardel[a,d,1]

[a]James Franck Institute, University of Chicago, Chicago, IL 60637; [b]Institute for Molecular Engineering, University of Chicago, Chicago, IL 60637; [c]Department of Physics, University of California, Merced, CA 95343; [d]Department of Physics, University of Chicago, Chicago, IL 60637; and [e]Department of Chemistry, University of Chicago, Chicago, IL 60637

Edited by Andrea J. Liu, University of Pennsylvania, Philadelphia, PA, and approved April 24, 2019 (received for review August 28, 2018)

The cytoskeleton is a collection of protein assemblies that dynamically impose spatial structure in cells and coordinate processes such as cell division and mechanical regulation. Biopolymer filaments, cross-linking proteins, and enzymatically active motor proteins collectively self-organize into various precise cytoskeletal assemblies critical for specific biological functions. An outstanding question is how the precise spatial organization arises from the component macromolecules. We develop a system to investigate simple physical mechanisms of self-organization in biological assemblies. Using a minimal set of purified proteins, we create droplets of cross-linked biopolymer filaments. Through the addition of enzymatically active motor proteins, we construct composite assemblies, evocative of cellular structures such as spindles, where the inherent anisotropy drives motor self-organization, droplet deformation, and division into two droplets. These results suggest that simple physical principles underlie self-organization in complex biological assemblies and inform bioinspired materials design.

active matter | liquid crystal | actomyosin | tactoids | spindle

Spontaneous organization occurs in biology at all length scales, from organelles and tissues to organisms and populations (1–3). For instance, during cell division, self-organized macromolecular assemblies drive localization of chromosomes to the cell midplane, segregate chromosomes, and split the cell into two daughter cells (4). Each stage relies on molecular species within the cytoplasm localizing precisely within space and time to regulate biochemical signals and generate mechanical stresses. While molecular self-organization principles have been intensely studied (3), we still lack understanding needed to reconstruct these intricate processes from purified components in vitro. Elucidating such principles would yield insights into in vivo regulation, as well as inform the design of novel, bioinspired, soft materials (5–8).

Biological molecules form unusual and adaptive machinery that drives physiological processes. The cytoskeleton, composed of biopolymer filaments and associated binding partners, constitutes a broad class of assemblies that regulate diverse processes ranging from cell motility and division to intracellular transport (9). A critical component of the cytoskeleton is actin, a protein which polymerizes into semiflexible filaments that assemble into elastic-like meshworks and bundles (10). These actin assemblies are responsible for regulating cell-shape changes and mechanics (10). Myosin II motors, found as bipolar filaments of a few hundred polymerized motors, drive relative motion of actin filaments, generating local force (11). When reconstituted in vitro, these assemblies exhibit striking dynamical behavior, where myosin motors drive the compaction and remodeling of actin networks (12).

In addition to the cytoskeleton, self-organized assemblies in the cytoplasm are ubiquitous. Liquid-like phases have been recently identified in a variety of proteins and nucleic acids (13, 14) and are thought to play important roles in subcellular compartmentalization (15). Macromolecular liquid droplets have also been proposed to have been the earliest primitive cells, or protocells, where reactive contents phase separated from the surrounding environment (16). These macromolecular droplets are thought of as isotropic liquids (13), characterized by a single viscosity and surface tension and lacking internal structure. We recently reported another type of macromolecular droplet, where the actin cross-linker, filamin, condenses short actin filaments into liquid droplets (17). While actin filament-based liquids have characteristics of conventional liquids, they are anisotropic due to internal structure from densely packed filaments, so instead form liquid crystals (17–19). The internal structure of molecular liquid crystals can be harnessed to drive processes such as spatial localization of colloidal particles (20, 21). Although the effect of active stresses generated by molecular motors in nematics is an emerging area of research (22–25), it is unknown in droplets and has no analog in experimental molecular liquid-crystal systems.

Here, we report macromolecular droplets, composed of actin liquid crystal embedded with the molecular motor myosin II, that robustly self-organize and spontaneously change shape. Intriguingly, these droplets exhibit two essential features of cell division: localization of species at the droplet midplane and droplet bisection into two "daughter" droplets. Using fluorescence microscopy, we find that individual myosin II filaments disperse throughout the actin droplet and migrate to the droplet midplane. Myosin filaments also form clusters that locally distort actin alignment and, when confined to droplets, drive droplet division into two daughter droplets of equal volume. We develop a continuum model, based on the alignment of rods in a structured fluid, to describe motor centering. By extending the model, through representing a motor cluster as a spherical colloid which favors radial alignment of actin, we capture droplet division. Of note, the data suggest that the role of enzymatic activity is to change the geometry of local actomyosin interactions, which we

Significance

Self-organized and shape-changing assemblies are fundamental in living systems. However, in synthetic materials, these features remain elusive to reconstruct. Here, we construct liquid droplets out of biological proteins actin and myosin, which are fundamental cellular materials. Since the proteins form filaments, the droplets have internal structure. This structure leads to the self-organization of the protein components, where myosin finds the center of actin droplets, reminiscent of chromosome alignment in cell division. Myosin also strongly interacts with actin, leading to spontaneous shape change and droplet division. These results suggest physical mechanisms of biological processes, while inspiring strategies for soft materials design.

Author contributions: K.L.W., K.D., S.V., and M.L.G. designed research; K.L.W. and K.D. performed research; K.L.W., K.D., T.A.W., and S.V. contributed new reagents/analytic tools; K.L.W. and K.D. analyzed data; and K.L.W., K.D., T.A.W., S.V., and M.L.G. wrote the paper.

The authors declare no conflict of interest.

This article is a PNAS Direct Submission.

[1]To whom correspondence may be addressed. Email: gardel@uchicago.edu.

This article contains supporting information online at www.pnas.org/lookup/suppl/doi:10.1073/pnas.1814854116/-/DCSupplemental.

Published online May 21, 2019.

represent as changes in colloid geometry in our model. Our results highlight that structural changes to droplets can be induced by colloidal objects, which potentially provides insight into physical mechanisms of center finding in biology and cell division, as well as informs the design of geometry-sensing and adaptive materials.

Results

To create structured actin droplets, we cross-link dilute (2.6 μM actin monomer), short (~200 nm) actin filaments with the actin-binding protein filamin (10 mol%; *SI Appendix*). Using confocal microscopy, we find that filamin quickly condenses short actin filaments into micrometer-sized spindle-shaped droplets, called tactoids (17). These droplets are composed of densely packed actin filaments surrounded by a vanishingly low bulk actin concentration (Fig. 1 *A* and *B*) (17). These droplets have properties of liquids, including an interfacial tension that determines their shape, growth through coalescence, and subunit diffusion (17). However, since the liquid is made of densely packed filaments, the filaments entropically align to form a nematic liquid crystal, where filaments have orientational order, giving rise to the tactoid shape (26, 27).

To investigate the effects of molecular motors in these structured droplets, we create composite actin droplets containing skeletal muscle myosin II. Under these conditions, the myosin polymerizes into filaments, where each filament has hundreds of individual myosin heads and is ~1 μm long and ~30 nm in diameter (28). Adding the cross-linker filamin to a solution of prepolymerized actin and myosin II induces the condensation of actin droplets embedded with myosin motors (Fig. 1*B*). These composite droplets have strikingly consistent features and shape, which are modulated by myosin concentration. For low myosin concentration, we observe that myosin punctae accumulate at the midplane of the droplet (Fig. 1*C* and Movie S1). The rod-like myosin puncta are near diffraction-limited in width and ~0.8–1.6 μm in length (*SI Appendix*, Fig. S1), consistent with individual myosin filaments. The rod-like puncta align with the tactoid long axis and stack across the droplet midplane. At higher myosin concentration, myosin II forms micrometer-sized clusters of myosin puncta. These clusters localize to droplet poles, while the droplet volume remains devoid of myosin (Fig. 1*D* and Movie S2). The myosin clusters either join two similarly sized actin droplets together ("bisected") or associate with isolated droplets ("separated") (Fig. 1*D* and Movie S2).

We use time-lapse fluorescence microscopy to explore the formation of bisected droplets. Although we miss the earliest droplet configuration, we find that isolated myosin puncta accumulate and cluster at the droplet midplane, over a few minutes (Fig. 1*E* and Movie S3; $t = 0$ is defined as the beginning of the movie). As myosin clusters accumulate, they become larger and rounder (*SI Appendix*, Fig. S1) and locally distort the actin droplet near the myosin cluster. This eventually leads to a single, micrometer-sized myosin cluster that distorts the droplet interface significantly enough to bisect the droplet into two smaller droplets (Fig. 1*F*). Bisected droplets are dynamic, where droplets occasionally spontaneously detach from the myosin cluster, yielding two individual, myosin-free droplets and an isolated myosin cluster with attached actin over ~1 min (Fig. 1*F* and Movies S4 and S5). Thus, actomyosin droplets exhibit spontaneous component centering and break up into two equal daughter droplets, reminiscent of active processes critical in biological cell division.

To investigate how composite droplet morphology varies with myosin concentration and enzymatic activity, we use two different methods to prepare myosin filaments with different levels of enzymatic activity and vary the concentration of motors. Stock solutions of myosin motors that have been frozen and thawed contain a significant proportion of motor domains that are inactive; that is, motors that bind to actin with high affinity and do not undergo a power stroke (low percent active motors) (*SI Appendix*) (29). To create myosin filaments containing a higher proportion of enzymatically active motors, a "clean-up" step after thawing is included to remove monomeric myosin that irreversibly bind to actin in the presence of high ATP (high percent active motors) (*SI Appendix*). At the lowest concentrations (2.4 nM), myosin prepared with a high percentage of active

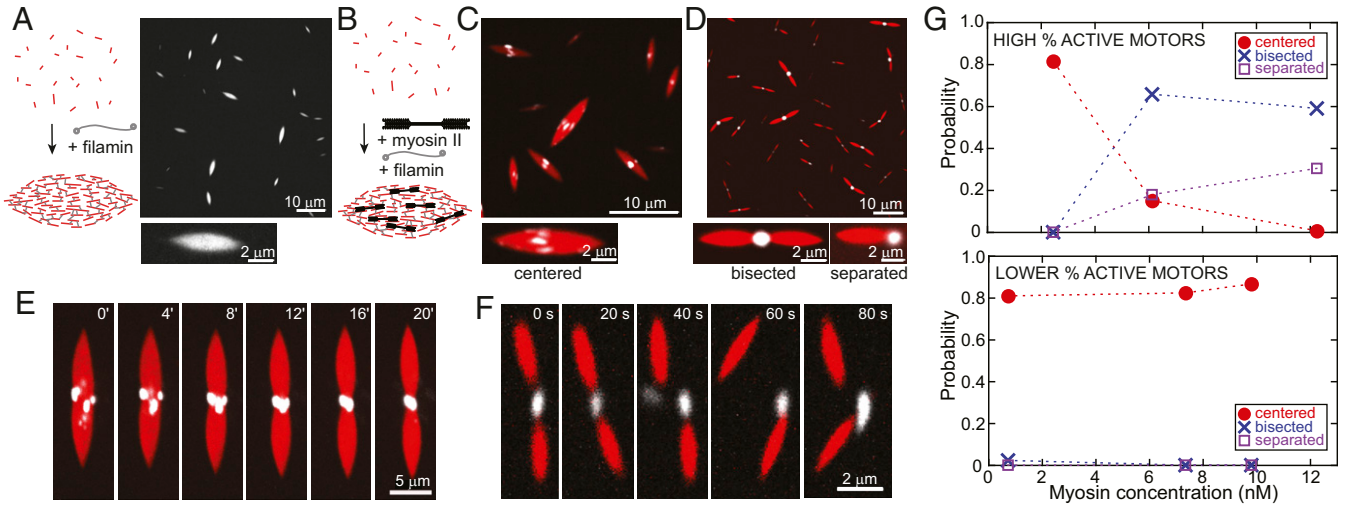

Fig. 1. Molecular motors self-organize and deform biopolymer droplets. (*A*) Cartoon of experimental system used to make actin droplets. Fluorescence images of filamin cross-linked short actin filaments condensed into droplets. (*B*) Cartoon of experimental system used to make actin droplets containing myosin filaments. (*C*, *Upper*) Fluorescence image of myosin II (white) organized at the midplane of actin droplets (red). (*C*, *Lower*) Close-up of single droplet with motors "centered." (*D*, *Upper*) Image of myosin II (white) clustered at the center of "bisected" droplets (red). (*D*, *Lower*) Close-up image of a bisected droplet, with the myosin cluster bridging droplets in a dimer and a "separated" droplet, where the myosin cluster localizes to the droplet pole. (*E*) Fluorescence images of myosin II puncta (white) migrating to the actin droplet (red) midplane as single rods, clustering, and bisecting the droplet (0 min defined as the beginning of data collection). (*F*) Image sequence of a motor cluster severing from actin droplets. (*G*) Distribution of actin–myosin droplet morphologies as a function of myosin concentration for a high proportion of active myosin motors (*Upper*) and low proportion of active motors (*Lower*), with fraction of centered, bisected, and separated morphologies observed.

heads exclusively center to the droplet midplane (Fig. 1*G*). As the myosin concentration increases beyond 6 nM, myosin prepared with a high percentage of active heads cluster and primarily form bisected droplets, with more separated droplets at the highest myosin concentration (Fig. 1*G*). To clarify how these structures depend on motor enzymatic activity, we perform experiments with a low fraction of active heads (*SI Appendix*). In these samples, myosin organize at the droplet midplane over all myosin concentrations, while rarely clustering in or dividing droplets (3 droplets divided in 280 droplets surveyed; Fig. 1*G* and Movie S6). This suggests that droplet bisection and separation are strongly dependent on motor enzymatic activity, whereas myosin centering is less so.

Myosin and Droplet Structure Drives Midplane Localization. The earliest droplets that we observe already have myosin at the midplane. Nevertheless, we can investigate the centering process by examining droplets shortly after they coalesce into a larger droplet (17). Immediately after coalescence of composite droplets, myosin is distributed throughout the droplet (Fig. 2*A* and Movie S7). Over minutes, myosin puncta migrate to the midplane (Fig. 2*A* and Movie S7). The probability distribution of myosin localization as a function of distance, d, from the droplet midplane normalized to its length, L_D, for 50 coalescence events indicates that this centered organization is general (Fig. 2*B*). Within 2 min of coalescence, ∼90% of myosin puncta are dispersed along the central 40% of the droplet long axis (Fig. 2 *A* and *B*). By 5 min, 65% of myosin puncta are at the midplane. Thus, myosin filaments initially located in distal droplet regions migrate to the droplet midplane.

To gain insight into the mechanism of myosin self-organization, we track the dynamics of individual myosin puncta. Tracking the normalized distance from the midplane, d/L_D, as a function of time suggests that myosin puncta initially located far from the midplane have steep trajectories directed toward the midplane, where $d/L_D = 0$ (Fig. 2*C*). By contrast, myosin initially located near the midplane undergo only small displacements (Fig. 2*C*). Taking the myosin speed to reflect the free-energy landscape, these data suggest that myosin at the droplet midplane have lower free energy compared with distal droplet locations. To quantify how myosin speed varies across the droplet, we extract the initial velocity from a linear fit to the early trajectory (Fig. 2 *C*, *Inset* and *SI Appendix*). Myosin puncta located near the midplane (d < 1.5 μm) have low initial speeds (∼1.4 nm/s), while their speeds increase to ∼6–10 nm/s when farther from the midplane (d > 2 μm) (Fig. 2*D*). These speeds are at least 100-fold slower than the unloaded gliding filament velocity of skeletal muscle myosin (30, 31). The low speeds indicate that actomyosin sliding is not likely responsible for myosin centering, consistent with our finding that centering occurs with reduced motor activity (Fig. 1*G, Lower*).

More than 90% of the centered myosin puncta align with the droplet major axis to within 10° (Fig. 2*E*). This is consistent with the known preference of myosin II filaments to bind to actin filaments, such that there is a high degree of alignment between their long axes (32). By sectioning the droplet midplane in z, we find that myosin are not only aligned, but also embedded throughout the bulk of the droplet, indicative of strong actin–myosin interactions (Fig. 2 *E*, *Inset*). Actin filament orientation varies spatially across the liquid-crystal droplet. Since we expect actin filaments to be splayed at the droplet poles and parallel to the droplet long axis near the midplane (Fig. 2*F*, cartoon; red lines indicate filament alignment) (33), we hypothesize that centering arises from the energetics of embedding the myosin rod in a structured actin droplet.

To gain further insight, we consider a continuum model where we model a single myosin II filament as an elongated rod of length L_M that interacts with orientationally aligned actin filaments in its vicinity. The myosin rod is embedded in a droplet with a long axis, $2L_D$, where a bipolar director configuration represents the local alignment of actin filaments. In this configuration, the curved director lines are parallel at the midplane and splayed near the droplet poles (Fig. 2*F*, cartoon, and *SI*

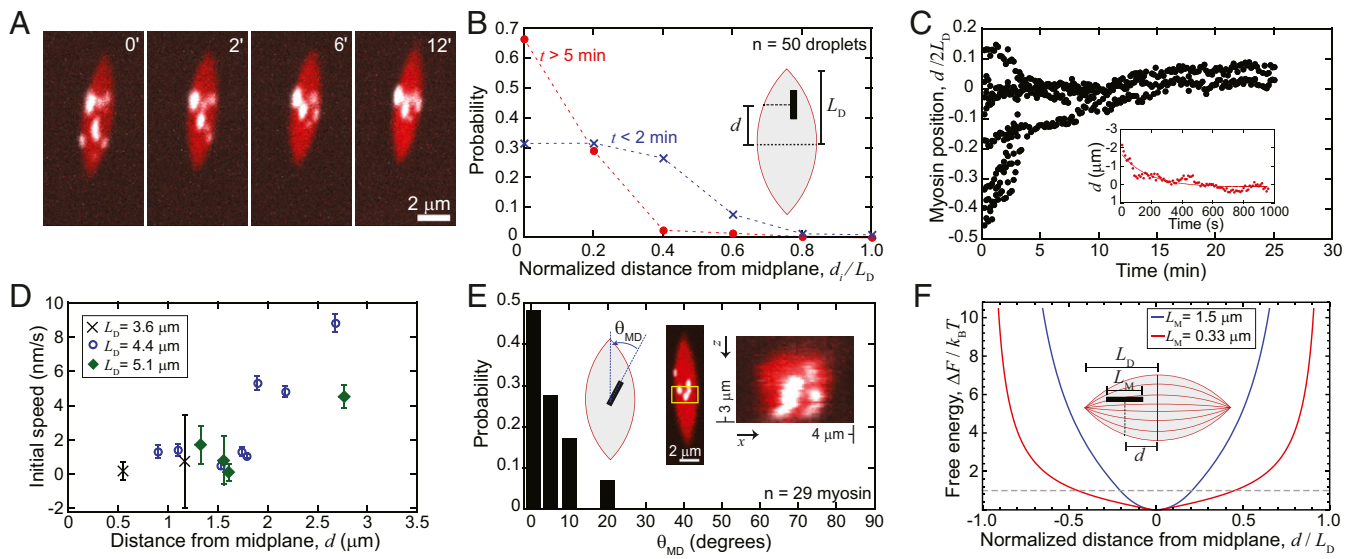

Fig. 2. Motors migrate to regions of minimum nematic splay. (*A*) Fluorescence microscopy image sequence of myosin II motors (white) in an actin droplet (red) (t = 0 min is defined as when tactoid reaches rest length after coalescence; Movie S7). (*B*) Probability distribution for motors along the droplet long axis, binned at regular intervals as a function of distance from the droplet midplane, normalized to the droplet length L_D (n = 50 droplets). (*C*) Myosin II puncta positions in the droplet in *A* over time. Distance is measured from the droplet midplane. Line is an exponential fit to the data. (*D*) Initial myosin II puncta speed as a function of initial distance from the droplet midplane for myosin in droplets with length 3.6 μm (black x's), 4.4 μm (blue open circles), and 5.1 μm (green diamonds). (*E*) Probability of alignment of myosin II puncta along droplet axis. (*E*, *Inset*) Fluorescence microscopy image of myosin II puncta aligned at midplane. Averaging over the region in yellow in y and projecting z indicate that myosin II puncta are distributed throughout the droplet bulk. (*F*) Continuum-model free-energy plots of two myosin puncta of different lengths as a function of their position within a tactoid of length, L_T = 3.2 μm. The free-energy scale in relation to k_BT is determined from the diffusive kinetics of centering puncta obtained from Fig. 2*D*.

Appendix, Fig. S2). Myosin II filaments are ∼30 nm wide, thin enough not to distort the surrounding actin nematic, in which we estimate a ∼50-nm spacing between actin filaments (17). We impose a strong orientational preference to represent the mutual alignment of myosin and actin filaments (32). Based on this geometry, we calculate the energetic cost of misalignment of the myosin rod, $\Delta F(d)$, expressed in terms of rod displacement, d, from the droplet midplane (*SI Appendix*). The resulting free-energy landscape of the rod has a minimum at the droplet midplane (Fig. 2*F*). As d increases, the rod interacts with more splayed directors, resulting in larger misorientation angles and higher energetic cost. For a longer rod (L_M = 1.5 μm; Fig. 2*F*, blue), the cost of misalignment is higher than for a shorter rod (L_M = 0.3 μm; Fig. 2*F*, red).

We consider whether thermal forces would be sufficient to drive motor rearrangements and consider the motors to be diffusive in the free-energy landscape, $\Delta F(d)$. We consider that a single motor filament experiences a centering force, $f(d)$, and use a harmonic approximation such that $f(d) = kd$, where k is the spring constant. The associated free energy, $\Delta F = kd^2/2$, may be written as $F_0 \cdot \left(\frac{d}{L_D}\right)^2$, where F_0 is approximately the work required to move a motor across the droplet. The centering speed, v, is determined by the equality of $f(d)$ and the drag force, Γv. The centering timescale of ∼10 min for motors near the midplane (Fig. 2*D*) is Γ/k. Although we expect that, like all structured fluids (34), the viscous drag is anisotropic, we use a previously estimated viscosity of actin tactoids, $\eta \sim 3$ Pa·s, which does not distinguish between anistropic components (17), to estimate the friction coefficient Γ, from which we obtain k and the corresponding energy scale, $F_0 \sim k\, L_D^2 \sim 10\, k_B T$ (*SI Appendix*). We then rescale the free-energy values with respect to thermal energy (Fig. 2*F*). The model predicts that the motor filaments drift toward the droplet midplane and center up to distances at which the centering energy becomes comparable to the thermal energy. We expect low centering speeds within a few micrometers of the midplane (Fig. 2*F*), consistent with experimental measurements of low velocities that are seemingly independent of d in that region (Fig. 2*D*). Thus, a model where rod-like myosin filaments center by optimizing their location within the structured actin droplet via thermally driven motion is consistent with our experimental data.

Myosin Clusters Deform and Divide Droplets via Disrupting Nematic Aligment. We next seek to understand how myosin localization at the droplet midplane results in droplet deformation. In the absence of myosin, actin droplets do not spontaneously divide (17), suggesting that myosin activity generates forces that counteract droplet interfacial tension and actin alignment to drive shape changes. In droplets containing myosin with a low proportion of active motors, myosin clusters and droplet distortion are only seen in 1% of droplets (n = 280 droplets), whereas clusters are seen in in 97% of droplets containing myosin with a higher proportion of active heads (n = 1,961 droplets). This suggests that the ability for myosin filaments to form clusters is related to enzymatic activity. Rod-like myosin filaments embedded within the actin droplet cause no local shape distortion or variation in the actin intensity (Fig. 3 *A*, *i*). Over time, myosin filaments rearrange into clusters, defined by their area and width (*SI Appendix*, Fig. S1). During clustering, puncta aggregate, increasing in area and becoming rounder (Fig. 3 *A*, *ii–iv* and *SI Appendix*, Fig. S1). Simultaneously, the droplet shape distorts at the myosin cluster location. Near large clusters, the amount of actin is depleted, as a precursor to droplet separation (Fig. 3 *A*, *iv*).

We propose that droplet distortions arise from changes in actin filament organization around myosin during clustering. Colloidal inclusions suspended in a nematic liquid crystal can distort and induce topological defects in the surrounding nematic (20). The nature of the distortion induced by a colloid depends on its size and anchoring, the preferential alignment of liquid-crystal constituents at the colloid surface. To investigate this, we examine the impact of myosin cluster shape and size on actin filament alignment in thin nematic layers of actin liquid crystals, where actin alignment is visible (*SI Appendix*) (23). In thin nematics, rod-like myosin puncta align parallel to actin filaments (Fig. 3 *B*, *i*). By contrast, myosin clusters impose local distortions in the nematic, such that actin filaments are canted around the cluster (Fig. 3 *B*, *ii–iv*), consistent with previous data showing that myosin clusters impose a radial arrangement of actin filaments (35).

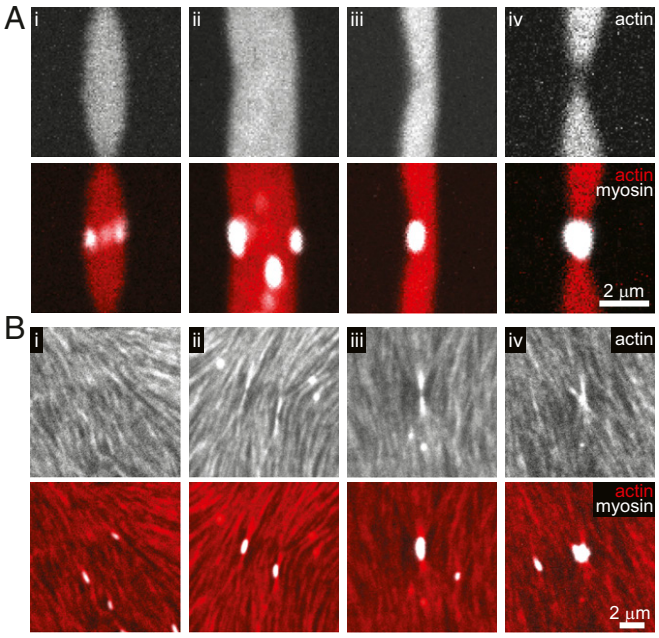

Fig. 3. Molecular motors distort actin alignment and induce droplet deformations. (*A*) Fluorescence images of actin (*Upper*) and actin and myosin (*Lower*; red, actin; white, myosin) in composite droplets. Individual myosin puncta do not visibly distort actin droplets (*A*, *i*), while small myosin puncta clusters distort the droplet interface (*A*, *ii* and *iii*), and large clusters divide droplets (*A*, *iv*). (*B*) Fluorescence images of an actin nematic, crowded to a thin (<1 μm) layer, showing actin (*Upper*) and actin and myosin (*Lower*; red, actin; white, myosin). Small myosin puncta align with the nematic (*B*, *i*), while larger myosin puncta and clusters distort the orientation of actin within the nematic (*B*, *ii–iv*). The scale bar applies to all images within each part (*A* and *B*).

Motivated by these experimental observations, we extend our continuum model to capture dividing droplets by representing the myosin cluster as a spherical colloid that imposes anchoring normal to its surface (Fig. 4*A*). In a bulk nematic, a colloid with normal anchoring creates defects in its vicinity (20, 21). In contrast to typical colloidal inclusions, myosin clusters bind to the surrounding actin, which we represent by an adhesion energy per unit area on the colloid surface, w. The bipolar droplet shape results from an optimization of the bulk nematic elastic and interfacial energies, with strong anchoring at the droplet interface (33). Since the myosin clusters impose normal anchoring, the radial convergence of the actin filaments near the droplet pole presents an optimal anchoring configuration. Like any liquid droplet, a single nematic droplet has lower interfacial energy than two such smaller droplets with the same total volume. However, we find that for droplets in contact with an adhesive colloid, the energetic gain from increased wetting of the colloid's surface counteracts the elastic and interfacial energetic cost of deforming the droplet, leading to the minimum configuration of a bisected droplet (*SI Appendix*). As the colloid size or adhesion

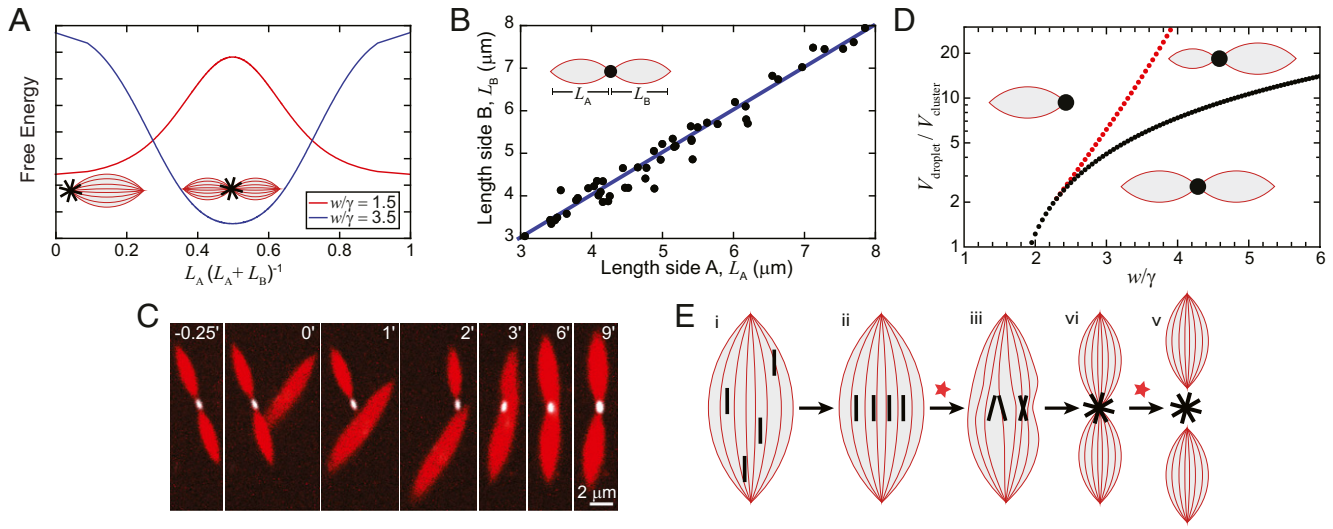

Fig. 4. Molecular motors bisect biopolymer droplets. (*A*) Total free energy from a continuum model of two droplets adhered to a colloid as a function of a droplet division parameter, $L_A \times (L_A + L_B)^{-1}$. Droplets are nematic and bipolar, with lengths L_A and L_B, and mechanical energy given by surface tension, γ, and the nematic elastic energy. Droplet length varies, while the total droplet volume is held constant. The colloid, which represents the motor cluster, has normal anchoring and adhesion energy per unit area, w. When w is large compared with the droplet mechanical energy, equal division of droplets is favorable (blue), while for lower w, a single droplet is favorable (red). Free-energy curves are normalized to display minima. While in this model, droplets are nearly spherical, similar qualitative behavior is calculated for very elongated bipolar droplets (*SI Appendix*). (*B*) Comparison of droplet length on either side of experimentally observed bisected droplets. Blue line indicates a slope of one. (*C*) Fluorescence images of an isolated droplet coalescing with a bisected droplet. (*D*) Phase space predicted by the continuum model of droplet division resulting from competition of droplet mechanical energy and adhesion with colloid (Fig. 4*A*). Black points indicate the boundary between a free-energy minimum and maximum in the equally divided state. Red points mark the transition between an unequal divided droplet, where one droplet is much smaller than the other, and a single whole droplet. (*E*) Cartoon summarizing motors in biopolymer droplets. Red stars indicate transitions where activity is hypothesized to be necessary.

strength increases compared with the droplet interfacial tension, the resulting adhesive energetic gain overwhelms the energetic cost of increasing the interface through shape distortions. In this case, two new droplet poles are created, and the motor cluster positions at the center of two, smaller droplets (Fig. 4 *A*, blue). While this equilibrium-bisected state requires both strong adhesion and anchoring, it is possible that the normal anchoring imposed by the colloid can distort the droplet into a long-lived, intermediate, bisected state before it relaxes to a different possible final configuration not observed within the experimental timescale. In contrast, when the adhesion is small compared with the interfacial tension, the droplet is not deformed, and the energetic minimum occurs when the colloid is at a droplet pole (Fig. 4 *A*, red), consistent with observations of colloids in nematic molecular liquid-crystal droplets (35), which have characteristically higher interfacial tension than the actin tactoids (17).

Droplets Prefer to Divide Equally. Strikingly, myosin clusters typically bisect droplets, with the resultant two droplets always apparently equal in size (Fig. 4*B*). Indeed, comparing the lengths on either side of a bisected dimer indicates that the motor cluster precisely divides the droplets into two equal droplets (Fig. 4*B*). The coalescence of a divided droplet dimer with an isolated droplet provides further evidence for the strong preference of droplet bisection (Fig. 4*C* and Movie S8). In this case, an isolated droplet coalesces with one droplet of the dimer, temporarily leading to the myosin cluster bridging two droplets of disparate sizes (Fig. 4*C*; 1–2 min). However, the actin redistributes over a few minutes until the droplets on either side of the myosin cluster are again equal. This indicates that the dimer with equal-sized droplets is a favored stationary configuration rather than a trapped state arising from the individual myosin puncta migrating to the droplet midplane before forming a cluster. Thus, adhesion from motor binding is large enough to favor redistribution of droplet material into two equal droplets.

We can theoretically explore how systematically changing the adhesion influences the preferred configuration of the actin droplet and myosin cluster. For low adhesion, the preferred configuration is a single large droplet with a myosin cluster at the pole. At intermediate adhesion, two droplets of unequal volume can form as a result of the competition between droplet interfacial energy and adhesion with colloid surface, while at higher adhesion, the two droplets are of equal volume (Fig. 4*D*).

Discussion

Here, we have introduced structured fluid droplets that exploit geometry sensing to generate spatial organization and drive shape change. While there are many potential manifestations of geometry sensing, we focus on droplets that exhibit essential aspects of cell division: center-finding and division into two identical daughters. The droplet shape evokes the mitotic spindle, and the center-finding is reminiscent of chromosome alignment at the spindle midplane. Our droplets comprise biomolecules quite distinct from those in the spindle, so similarilities highlight potentially shared physical mechanisms. In fact, spindle shape and dynamics are captured by the physics of active structured fluids (25). While structured fluids, such as molecular liquid crystals, have long been used to organize colloids at defects and interfaces (20, 21, 36–39), here, we exploit colloid affinity to the liquid constituents to change the energetically favored locations within the liquid-crystal bulk. This interplay of adhesion, interfacial tension, and elasticity potentially has implications in regulation of spatial organization in subcellular liquid droplets beyond the spindle, in primitive and synthetic cells, and other macromolecular droplets such as coacervates (25, 40–42). In the future, this system can be extended to elucidate how colloid adhesion and shape, together with fluid structure, direct spatiotemporal organization in structured fluids, which may inform the design of novel structured, soft materials.

A key feature of biological cells that remains elusive to reconstruct in synthetic systems is cell division (42, 43). Driving droplet shape changes has an energetic penalty associated with increasing the amount of droplet interface due to an interfacial tension. Typically, activity is invoked in theoretical arguments to provide the energy associated with deforming the interface (16, 44, 45). By contrast, here, we demonstrate a mechanism by which droplet division can occur passively, as a mechanical equilibrium state resulting from the competition between colloid adhesion with the droplet and the droplet energetics (Fig. 4*E*). Droplet division has also been theoretically proposed to be mediated by liquid-crystal defects for a droplet geometry and anchoring distinct from this system (46). Our model of passive rods in a structured droplet captures the key observation that myosin filaments center, even with reduced enzymatic activity (Fig. 4 *E*, *i* and *ii*). Although our proposed model indicates that droplet and colloid geometry are key factors in driving the localization of motor proteins, it does not exclude the possible contributions of motor activity in our experiment. Likewise, the passive model of an adhesive colloid with radial anchoring is sufficient to capture the preference for a droplet to form two equal droplets attached to the colloid (Fig. 4 *E*, *iv*). We hypothesize that enzymatic activity is key to regulate changes in colloid shape and binding interactions, in this system manifesting as the changes in myosin geometry during clustering (Fig. 4 *E*, *iii*, active contribution indicated by red star). We also hypothesize that activity is key to the complete separation of bisected droplets (Fig. 4 *E*, *v*, red star).

While the fluid structure in molecular liquid crystals is used to spatially organize colloids in droplets (21, 38, 39), our research suggests colloidal wetting as a strategy to drive droplet deformations. In particular, we present a robust approach to drive droplet division into two equal daughters. In lyotropic systems such as these actin-based droplets, the entropic effects are much more prominent compared with molecular liquid crystals due to the longer lengths of the nematogens (actin filaments) and colloids (myosin filaments). This different length scale may be critical to using colloids to drive shape changes. An exciting area of future research will be to utilize large, macromolecular liquids and chemical activity based on these mechanisms to sense geometry, robustly organize, and induce deformations to create novel, adaptive soft materials.

Methods

To prepare composite structured droplets, we add 10 mol% filamin cross-linker to 2.6 μM actin, polymerized into ∼200-nm filaments, where filament length is regulated by capping protein (1.5 mol%), in the presence of skeletal muscle myosin II. To prepare thin nematic actin layers, we add 1.1 nM skeletal muscle myosin II to a layer of actin filaments (2.6 μM, 1.2 mol% capping protein) crowded at a passivated surface by 0.4 wt% methylcellulose. Details of all methods can be found in *SI Appendix*.

ACKNOWLEDGMENTS. We thank T. Thoresen and S. Stam for purified filamin; S. Stam for myosin; C. Suarez for advising the purification of capping protein; and J. Vieregg, D. Coursault, R. Zhang, and P. van der Schoot for inspiring and insightful discussions. This research was primarily supported by the University of Chicago Materials Research Science and Engineering Center (NSF Division of Materials Research Grant 1420709). Additional support was provided by a Sloan Fellowship (to S.V.); Army Research Office Multidisciplinary University Research Initiatives Grant W911NF1410403; NSF Grant 1344203; and NIH Grant R01 GM104032 (to M.L.G.).

1. X. Trepat, E. Sahai, Mesoscale physical principles of collective cell organization. *Nat. Phys.* **14**, 671–682 (2018).
2. M. C. Marchetti *et al*., Hydrodynamics of soft active matter. *Rev. Mod. Phys.* **85**, 1143–1189 (2013).
3. E. Karsenti Self-organization in cell biology: A brief history. *Nat. Rev. Mol. Cell Biol.* **9**, 255–262 (2008).
4. B. Alberts *et al*., *Molecular Biology of the Cell* (Garland Science, New York, ed. 6, 2015).
5. R. Merindol, A. Walther, Materials learning from life: Concepts for active, adaptive and autonomous molecular systems. *Chem. Soc. Rev.* **46**, 5588–5619 (2017).
6. H. Shahsavan, L. Yu, A. Jákli, B. Zhao, Smart biomimetic micro/nanostructures based on liquid crystal elastomers and networks. *Soft Matter* **13**, 8006–8022 (2017).
7. S. Palagi, P. Fischer, Bioinspired microrobots. *Nat. Rev. Mater.* **3**, 113–124 (2018).
8. G. Zan, Q. Wu, Biomimetic and bioinspired synthesis of nanomaterials/nanostructures. *Adv. Mater.* **28**, 2099–2147 (2016).
9. L. Blanchoin, R. Boujemaa-Paterski, C. Sykes, J. Plastino, Actin dynamics, architecture, and mechanics in cell motility. *Physiol. Rev.* **94**, 235–263 (2014).
10. C. P. Broedersz, F. C. MacKintosh, Modeling semiflexible polymer networks. *Rev. Mod. Phys.* **86**, 995–1036 (2014).
11. M. Murrell, P. W. Oakes, M. Lenz, M. L. Gardel, Forcing cells into shape: The mechanics of actomyosin contractility. *Nat. Rev. Mol. Cell Biol.* **16**, 486–498 (2015).
12. F. Backouche, L. Haviv, D. Groswasser, A. Bernheim-Groswasser, Active gels: Dynamics of patterning and self-organization. *Phys. Biol.* **3**, 264–273 (2006).
13. A. A. Hyman, C. A. Weber, F. Juelicher, "Liquid-liquid phase separation in biology" in *Annual Review of Cell and Developmental Biology*, R. Schekman, R. Lehmann, Eds. (Annual Reviews, Palo Alto, CA, 2014), **vol. 30**, pp. 39–58.
14. Y. Shin, C. P. Brangwynne, Liquid phase condensation in cell physiology and disease. *Science* **357**, 1253 (2017).
15. C. P. Brangwynne *et al*., Germline P granules are liquid droplets that localize by controlled dissolution/condensation. *Science* **324**, 1729–1732 (2009).
16. D. Zwicker, R. Seyboldt, C. A. Weber, A. A. Hyman, F. Julicher, Growth and division of active droplets provides a model for protocells. *Nat. Phys.* **13**, 408–413 (2017).
17. K. L. Weirich *et al*., Liquid behavior of cross-linked actin bundles. *Proc. Natl. Acad. Sci. U.S.A.* **114**, 2131–2136 (2017).
18. R. Zhang, N. Kumar, J. L. Ross, M. L. Gardel, J. J. de Pablo, Interplay of structure, elasticity, and dynamics in actin-based nematic materials. *Proc. Natl. Acad. Sci. U.S.A.* **115**, E124–E133 (2018).
19. J. Viamontes, P. W. Oakes, J. X. Tang, Isotropic to nematic liquid crystalline phase transition of F-actin varies from continuous to first order. *Phys. Rev. Lett.* **97**, 118103 (2006).
20. I. I. Smalyukh, Liquid crystal colloids. *Annu. Rev. Condens. Matter Phys.* **9**, 207–226 (2018).
21. P. Poulin, H. Stark, T. C. Lubensky, D. A. Weitz, Novel colloidal interactions in anisotropic fluids. *Science* **275**, 1770–1773 (1997).
22. T. Sanchez, D. T. N. Chen, S. J. DeCamp, M. Heymann, Z. Dogic, Spontaneous motion in hierarchically assembled active matter. *Nature* **491**, 431–434 (2012).
23. N. Kumar, R. Zhang, J. J. de Pablo, M. L. Gardel, Tunable structure and dynamics of active liquid crystals. *Sci. Adv.* **4**, t7779 (2018).
24. J. Prost, F. Julicher, J. F. Joanny, Active gel physics. *Nat. Phys.* **11**, 111–117 (2015).
25. J. Brugués, D. Needleman, Physical basis of spindle self-organization. *Proc. Natl. Acad. Sci. U.S.A.* **111**, 18496–18500 (2014).
26. P. G. de Gennes, J. Prost, *The Physics of Liquid Crystals* (Claredon Press, Oxford, 1993).
27. P. Prinsen, P. van der Schoot, Continuous director-field transformation of nematic tactoids. *Eur. Phys. J. E. Soft Matter* **13**, 35–41 (2004).
28. T. Thoresen, M. Lenz, M. L. Gardel, Thick filament length and isoform composition determine self-organized contractile units in actomyosin bundles. *Biophys. J.* **104**, 655–665 (2013).
29. J. Howard, *Mechanics of Motor Proteins and the Cytoskeleton* (Sinauer Associates, Sunderland, MA, 2001).
30. J. A. Spudich, S. J. Kron, M. P. Sheetz, Movement of myosin-coated beads on oriented filaments reconstituted from purified actin. *Nature* **315**, 584–586 (1985).
31. S. J. Kron, J. A. Spudich, Fluorescent actin filaments move on myosin fixed to a glass surface. *Proc. Natl. Acad. Sci. U.S.A.* **83**, 6272–6276 (1986).
32. H. F. Epstein, D. A. Fischman, Molecular analysis of protein assembly in muscle development. *Science* **251**, 1039–1044 (1991).
33. P. Prinsen, P. van der Schoot, Shape and director-field transformation of tactoids. *Phys. Rev. E. Stat. Nonlin. Soft Matter Phys.* **68**, 021701 (2003).
34. M. Miesowicz, The three coefficients of viscosity of anisotropic liquids. *Nature* **158**, 27 (1946).
35. S. Stam *et al*., Filament rigidity and connectivity tune the deformation modes of active biopolymer networks. *Proc. Natl. Acad. Sci. U.S.A.* **114**, E10037–E10045 (2017).
36. M. Cavallaro, Jr, L. Botto, E. P. Lewandowski, M. Wang, K. J. Stebe, Curvature-driven capillary migration and assembly of rod-like particles. *Proc. Natl. Acad. Sci. U.S.A.* **108**, 20923–20928 (2011).
37. C. Blanc, D. Coursault, E. Lacaze, Ordering nano- and microparticles assemblies with liquid crystals. *Liq. Cryst. Rev.* **1**, 83–109 (2013).
38. X. Wang, D. S. Miller, J. J. de Pablo, N. L. Abbott, Organized assemblies of colloids formed at the poles of micrometer-sized droplets of liquid crystal. *Soft Matter* **10**, 8821–8828 (2014).
39. M. Rahimi *et al*., Nanoparticle self-assembly at the interface of liquid crystal droplets. *Proc. Natl. Acad. Sci. U.S.A.* **112**, 5297–5302 (2015).
40. A. B. Marciel, E. J. Chung, B. K. Brettmann, L. Leon, Bulk and nanoscale polypeptide based polyelectrolyte complexes. *Adv. Colloid Interface Sci.* **239**, 187–198 (2017).
41. M. J. York-Duran *et al*., Recent advances in compartmentalized synthetic architectures as drug carriers, cell mimics and artificial organelles. *Colloids Surf. B Biointerfaces* **152**, 199–213 (2017).
42. F. Caschera, V. Noireaux, Integration of biological parts toward the synthesis of a minimal cell. *Curr. Opin. Chem. Biol.* **22**, 85–91 (2014).
43. V. Noireaux, Y. T. Maeda, A. Libchaber, Development of an artificial cell, from self-organization to computation and self-reproduction. *Proc. Natl. Acad. Sci. U.S.A.* **108**, 3473–3480 (2011).
44. C. A. Whitfield, R. J. Hawkins, Instabilities, motion and deformation of active fluid droplets. *New J. Phys.* **18**, 123016 (2016).
45. L. Giomi, A. DeSimone, Spontaneous division and motility in active nematic droplets. *Phys. Rev. Lett.* **112**, 147802 (2014).
46. M. Leoni, O. V. Manyuhina, M. J. Bowick, M. C. Marchetti, Defect driven shapes in nematic droplets: Analogies with cell division. *Soft Matter* **13**, 1257–1266 (2017).